The optical properties of tellurium under high pressure

1995 J. Phys.: Condens. Matter 7 4299

(http://iopscience.iop.org/0953-8984/7/22/012)

J. Phys.: Condens. Matter 7 (1995) 4299–4312. Printed in the UK

The optical properties of tellurium under high pressure

Itsuro Yamamoto, Yoshinori Ohmasa, Hiroshi Ikeda and Hirohisa Endo†
Department of Physics, Faculty of Science, Kyoto University, Kyoto 606-01, Japan

Received 17 October 1994, in final form 10 February 1995

Abstract. Reflectivity spectra of Te have been measured in the energy range from 0.5 to 3.8 eV at pressures up to 96 kbar using a diamond anvil cell. Optical conductivity spectra $\sigma(\omega)$ have been derived from the reflectivity by using an oscillator fitting analysis. The $\sigma(\omega)$ spectrum for trigonal Te at 1 kbar has a main peak at 2.2 eV and a shoulder around 1.2 eV. These peaks shift to lower energy and grow with increasing pressure. When Te is transformed into a monoclinic phase around 40 kbar, a Drude term appears in the low-energy region of the $\sigma(\omega)$ spectrum, which suggests that monoclinic Te has a metallic nature. In the orthorhombic phase at 73 kbar, a main peak at 0.5 eV and a shoulder around 1.2 eV are observed for the $\sigma(\omega)$ spectrum. These changes in the $\sigma(\omega)$ spectra of Te with pressure are discussed in comparison with the results of band calculations.

1. Introduction

It is well known that tellurium (Te) exhibits various structural phase transitions under pressure. Trigonal Te, the stable form under ambient conditions, is characterized by a crystal structure with spiral chains parallel to the c axis as shown in figure 1(a). Its space group is D_3^4 or D_3^6 depending on the direction of screw axes along the chains. Each atom is tightly bonded to two neighbours in a chain with covalent bonds. On the other hand, the bonding between neighbouring chains is much weaker.

Many investigations have been done for the determination of the structure of Te under high pressure [1–5]. Figure 2 shows the recent results measured by Ohmasa *et al* [6] for the pressure variation of the lattice constants of trigonal Te. The a axis perpendicular to the chains contracts substantially with pressure up to 40 kbar, while the c axis parallel to the chains elongates slightly. When the distance between neighbouring chains is reduced by applying pressure, the spiral chain conformation is modified. In fact, trigonal Te is transformed into a monoclinic phase (space group C_2^2) at 40 kbar, which is characterized by a puckered layer structure with four atoms per unit cell as shown in figure 1(b) [5]. Each layer consists of planar zig-zag chains extending along the c direction in the bc plane. The zig-zag chains are composed of alternating short bonds (2.80 Å) and long bonds (3.10 Å) and are stacked in the a-axis direction. As a result, each atom has four nearest neighbours in the layer. The angle β between the a axis and the c axis is 92.7° at 45 kbar. With further pressure up to 68 kbar, monoclinic Te undergoes the structural phase transition to an orthorhombic phase. Orthorhombic Te consists of the same puckered layer structure as monoclinic Te, except that the bond lengths of the short bonds and the long bonds become the same (3.04 Å) and the angle β is equal to 90° [5, 6]. Figure 3 shows the pressure variation of the lattice constants for monoclinic Te and orthorhombic Te [5, 6]. The b axis

† Present address: Faculty of Engineering, Fukui Institute of Technology, Fukui 910, Japan.

0953-8984/95/224299+14$19.50

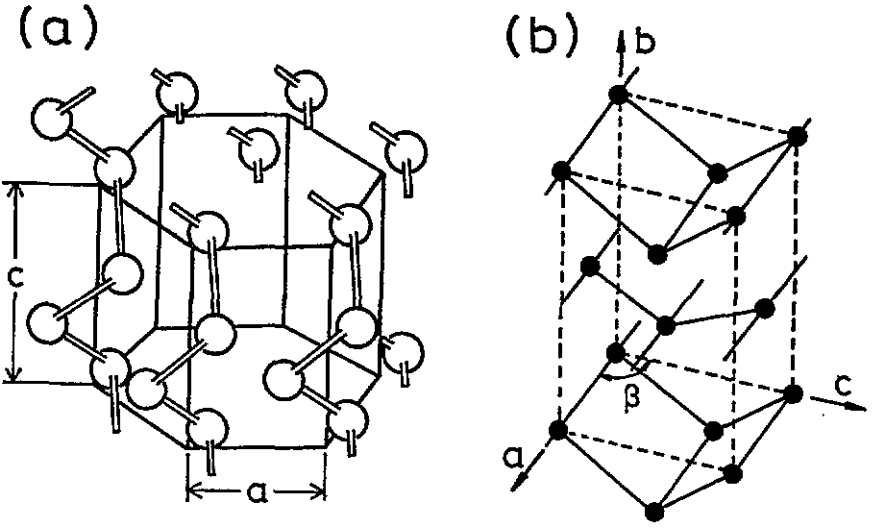

Figure 1. Crystal structures of (a) trigonal Te and (b) monoclinic Te.

contracts greatly with increasing pressure, while the changes of the c axis and the a axis are rather small. Orthorhombic Te is transformed into a β-Po-type structure (space group D_{3d}^5) at 110 kbar. Furthermore, Parthasarathy and Holzapfel [4] have reported that the phase transition to a body-centred cubic (BCC) structure is observed at 270 kbar.

It should be noted that the electronic states of Te are closely related to the structure. The atomic configuration of Te is $5s^25p^4$. In the trigonal phase two of the 5p electrons form σ bonding orbitals and the other two occupy non-bonding lone-pair (LP) orbitals, which form the highest valence band, while empty σ^* antibonding orbitals form the conduction band. Therefore, trigonal Te exhibits semiconducting behaviour with a narrow band gap of 0.33 eV. The LP orbitals face the σ^* orbitals in the neighbouring chain, which causes charge transfer between the orbitals, and the repulsive exchange interaction between LP orbitals plays an important role in stabilizing the spiral chain structure. The band calculations for semiconducting trigonal Te under pressure have been carried out by Starkloff and Joannopoulos [7, 8] using a self-consistent pseudopotential method and by Isomaki *et al* [9, 10] using a self-consistent Hartree–Fock–Slater method. According to them, all bands broaden with increasing pressure. They also predicted that the band gap narrows and the LP to σ^* optical transitions appear at lower energies under pressure.

The phase transition of Te from trigonal to monoclinic structure is accompanied by the electronic transition to the metallic state. Electrical resistance measurements have confirmed that the high-pressure phases above 40 kbar are metallic and become superconducting at low temperature [6, 11–15]. The band calculations for monoclinic Te have been done independently by Doerre and Joannopoulos [16] using a self-consistent pseudopotential method and by Shimoi and Fukutome [17] using a vector charge-density-wave method. It was found that some bands cross the Fermi level along the Γ to X direction, and no bands cross along the Γ to Y direction or the Γ to Z direction, which suggests that the conduction is extremely anisotropic, i.e. the conductivity along the *a*-axis direction is metallic, while that along the *bc* plane parallel to the zig-zag covalent chains is semiconducting.

It is very interesting to elucidate how the structural changes of Te induced by pressure are reflected on the electronic states. However, no experimental data are available for the electronic states under pressure at the present stage. Reflectivity data provide very useful

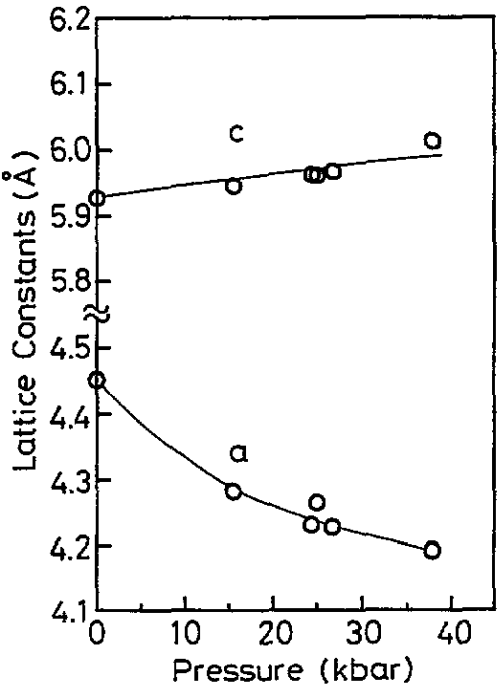

Figure 2. Pressure variation of lattice constants a and c for trigonal Te [6].

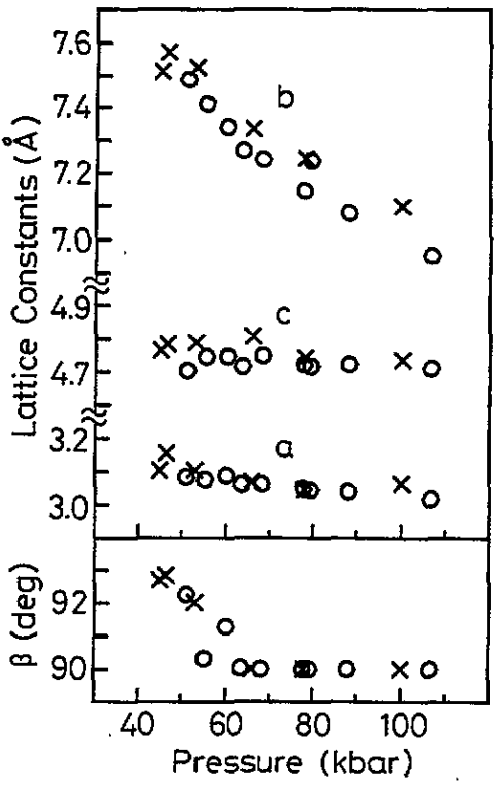

Figure 3. Pressure variation of lattice constants and the angle β between the a axis and the c axis for monoclinic Te and orthorhombic Te. Open circles represent the recent data measured by Ohmasa *et al* [6] and crosses the data taken from [5].

information on the electronic states. In this paper we report reflectivity spectra of Te at pressures up to 96 kbar and at room temperature. The reflectivity spectra were analysed using an oscillator fitting method, and optical conductivity spectra were derived.

2. Experiment and data analysis

2.1. Sample preparation

A diamond anvil cell was used to generate pressures up to 96 kbar. Figure 4 shows the interior assembly of the high-pressure cell. Diamond anvils have central flats of 1 mm diameter. Te powder (99.999% purity) was placed inside an Inconel gasket hole of 300 μm diameter and was in direct contact with the upper diamond. A high-polymer film was used as the pressure medium, which was set between the sample and the lower diamond. Ag films (99.98% purity) 20 μm thick were inserted between the upper diamond and the gasket as seen in the figure, to determine the absolute value of reflectivity.

Reflectivity was measured at the diamond–sample interface. For the measurements at relatively low pressures below 10 kbar, special care was taken to get a flat surface of the sample. After the sample was pressed above 10 kbar in advance, the measurements of the

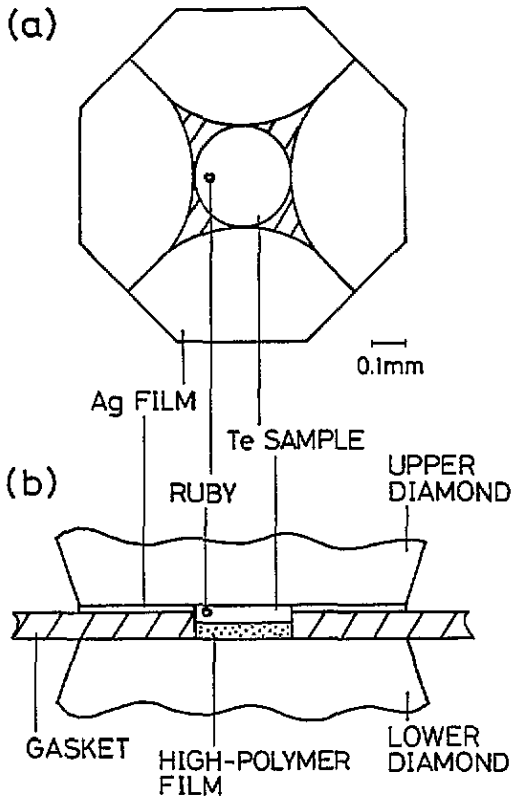

Figure 4. Interior assembly of the high-pressure cell for reflectivity measurements. Incident and reflected light pass through the upper diamond.

reflectivity were carried out by slowly releasing the pressure. Thus, optical constants of Te at 1 kbar obtained in this way are in agreement with the literature data of single-crystal Te in vacuum as described later. A diamond of type Ia was used, so that the measured energy range was restricted from 0.5 to 4.0 eV [18]. It has been reported that the reflectivity of Ag is nearly structureless and independent of pressure in the energy range below the 'plasma edge' [19]. This implies that Ag film can be useful as a reference sample in the energy range 0.5–3.8 eV. Pressure was determined by measuring the fluorescence from a chip of ruby placed in the gasket hole.

2.2. *Micro-optical system*

Since the size of the sample set in the diamond anvil cell is 300 μm in diameter, a special optical apparatus is needed to measure reflection spectra from such a micro-sample. Micro-optical devices have been reported already by Welber [20, 21] and Syassen and Sonnenschein [19]. The micro-optical system designed by us for reflectivity measurements under pressure is shown in figure 5.

The light from a tungsten halogen lamp (50 W) was collected with a fused silica lens (biconvex type, $f = 38$ mm), and focused on the aperture of a pinhole (100 μm in diameter). The image of this aperture was focused onto the sample in the cell by a spherical mirror ($r = 250$ mm) and a beam splitter (a fused silica plate coated with Cr), which was set

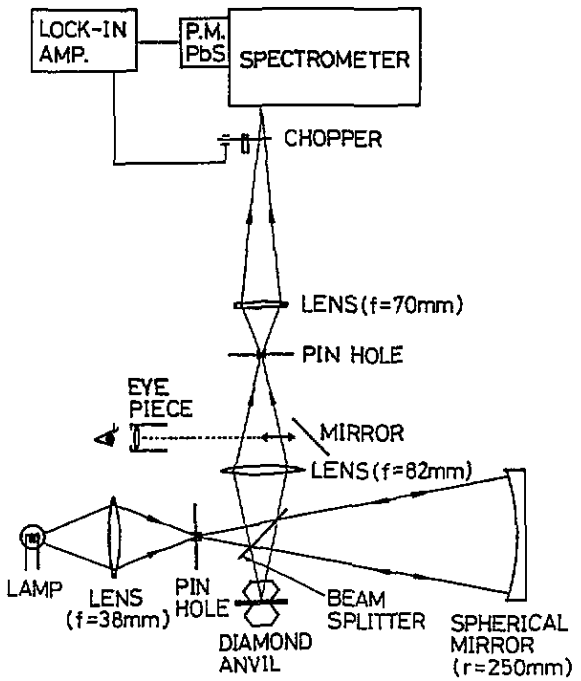

Figure 5. Schematic drawing of the micro-optical system for reflectivity measurements under pressure.

at 45°. The diamond cell was mounted on an x–y–z stage with micrometers. The image on the sample was adjusted to the same size as the aperture with little coma and spherical aberration.

The reflected light from the sample was collected with a fused silica lens (biconvex type, $f = 82$ mm), and focused on a second pinhole (about 2 mm in diameter). By a slight shift of the optic axis, this pinhole blocks the direct light from the first aperture, which is reflected by the beam splitter. We can observe directly the image on the sample through an eyepiece, when a mirror is inserted between the second pinhole and the lens. The reflected light passing through the second pinhole was magnified about 10 times by a fused silica lens (planoconvex type, $f = 70$ mm), and focused on the entrance slit of a spectrometer (Shimadzu, UV-365). A chopper was set in front of the slit.

The monochromatic light was detected by a thermoelectrically cooled PbS cell or a photomultiplier, and the signal was fed into a lock-in amplifier (EG&G, model 5208). At every measurement the spectrometer was scanned at energy intervals of 0.05 eV in the energy range from 0.5 to 4.0 eV. At each energy the signals from the lock-in amplifier were integrated and averaged in a microcomputer.

It should be noted that all reflection spectra shown in this paper give the reflectivity against a diamond window, that is

$$R = \frac{(n - n_{\mathrm{dia}})^2 + k^2}{(n + n_{\mathrm{dia}})^2 + k^2}. \tag{1}$$

Here n and k are the refractive index and extinction coefficient of the sample, respectively, and n_{dia} is the refractive index of diamond [18]. The reflectivity of the sample was calculated

from the ratio of two reflected intensities, namely the reflected intensity from the sample and that from the reference sample (Ag film). The reflectivity of the Ag film against a diamond window was estimated in advance. In our micro-optical system the reflected light from the air–diamond interface in addition to that from the sample is also included. Hence the reflectivity was corrected for the reflection at the air–diamond interface by using the reflectivity of diamond calculated from its refractive index.

2.3. Oscillator fitting method

To derive optical constants from reflectivity spectra, a Kramers–Kronig method is usually used. However, the measured energy range, which is restricted by the cut off energy of diamond, is too narrow to apply the Kramers–Kronig method. An alternative method, namely an oscillator fitting method, was used in the present study. The method consists of an iterative procedure adjusting the parameters of a classical oscillator model to fit the reflectivity data. Recently this technique has been applied with success to analyse the reflectivity of liquid chalcogen under high temperature and high pressure [22].

We assume the following dielectric function:

$$\varepsilon(\omega) = \varepsilon_1(\omega) - \mathrm{i}\varepsilon_2(\omega) = \varepsilon_\infty - \frac{\omega_p^2}{\omega^2 - \mathrm{i}\omega\Gamma_0} + \sum_j \frac{S_j\omega_j^2}{\omega_j^2 - \omega^2 + \mathrm{i}\omega\Gamma_j}. \tag{2}$$

Here ω_j, Γ_j and S_j are the angular frequency, width and strength of the jth oscillator respectively; ε_∞ is the contribution of high-frequency excitations to the dielectric function; ω is the light angular frequency; and ω_p and Γ_0 represent the contribution from free electrons within the Drude model. The second term on the right-hand side of equation (2) is the so-called Drude term which appears in the metallic phase. Optical conductivity is given by

$$\sigma(\omega) = (\omega/4\pi)\varepsilon_2(\omega). \tag{3}$$

The optical conductivity $\sigma(0)$ for $\omega = 0$ represents the DC conductivity.

We determined the parameters in equation (2) in such a way that the calculated reflectivity fits the measured spectra. The reflectivity spectra vary smoothly over the entire energy range, and neither fine structure nor a steep change of the reflectivity is observed as shown later. Hence oscillators with constant Γ_j of 0.4 eV were set at regular energy intervals of 0.2 eV in the energy range 0 to 6 eV. Then the quantities ε_∞ and S_j were chosen as adjustable parameters. In this case the values of ω_j, Γ_j and S_j of the individual oscillator make no physical sense. At the end of the fitting process the relative difference between the calculated and measured values of the reflectivity was less than a few per cent over the entire energy range. However, despite the very good correspondence between calculated and experimental data, it must be pointed out that fitting a multiparameter model to a curve spanning a relatively narrow energy range can yield non-unique answers. In order to extract the correct set of dielectric constants, this analysis needs additional information. For trigonal Te we used as additional constraints the values of the energy gap obtained from the temperature dependence of electrical resistance under pressure [13]. For monoclinic phase and orthorhombic phase the values of DC conductivity estimated from our electrical resistance measurements were used, i.e. $\sigma(0) = 2000\ \Omega^{-1}\ \mathrm{cm}^{-1}$ for monoclinic phase and $\sigma(0) = 2500\ \Omega^{-1}\ \mathrm{cm}^{-1}$ for orthorhombic phase [6].

An example for the quality of fit is given in figure 6(a). The dotted curve denotes the reflectivity spectrum measured at 1 kbar, and the full curve denotes its fitting curve. The

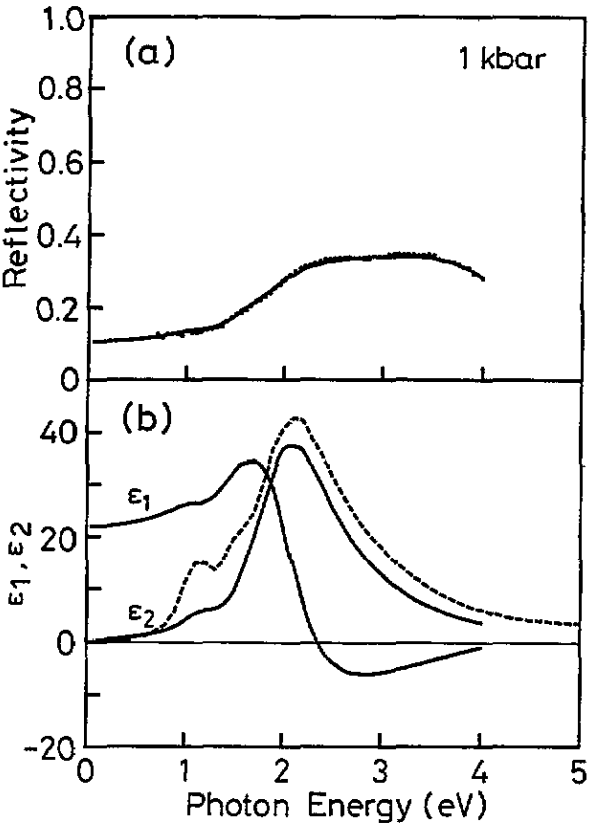

Figure 6. (a) Reflectivity spectrum of Te at 1 kbar (dotted curve) and its fitting curve (full curve). (b) The ε_1 and ε_2 spectra derived by using an oscillator fitting method. The broken curve indicates the average of $\varepsilon_{2\parallel}$ ($E \| c$) and $\varepsilon_{2\perp}$ ($E \perp c$) obtained for a single crystal of trigonal Te [23]. The average was calculated according to $(\varepsilon_{2\parallel} + 2\varepsilon_{2\perp})/3$.

ε_1 and ε_2 spectra derived from the fitting curve are shown by full curves in figure 6(b). In the ε_2 spectrum we observe a main peak at 2.1 eV and a small subpeak around 1.2 eV. Tutihasi *et al* [23] have measured the reflectivity spectra of single-crystal Te in vacuum up to the vacuum-ultraviolet region and have derived ε_1 and ε_2 spectra by using the Kramers–Kronig method. Their ε_2 spectrum is shown by the broken curve in figure 6(b). The whole shape of our ε_2 spectrum and the peak positions of the main peak and the subpeak are in good agreement with their data, though the subpeak in our ε_2 spectrum is less pronounced. Examples for the quality of fits at other pressures are shown later.

3. Results

3.1. Reflectivity spectra

Figure 7 shows the pressure variation of the reflectivity spectra of Te up to 96 kbar. It should be noted that the zero lines of the reflectivity are shifted upwards by 0.1 for each different pressure. Te at pressures from 1 to 38 kbar, from 42 to 60 kbar and from 73

to 96 kbar exhibits the trigonal phase, the monoclinic phase and the orthorhombic phase respectively†. Each phase has anisotropic crystal structures as described in section 1. Since powdered polycrystalline Te was used in the present study, all spectra in figure 7 give a reflectivity whose anisotropy was averaged out. The reflectivity spectra show smoothed curves, though data points below 1.0 eV and above 3.6 eV are slightly scattered owing to the weakness of the reflected intensity. These spectra were reproducible within experimental error in repeated measurements.

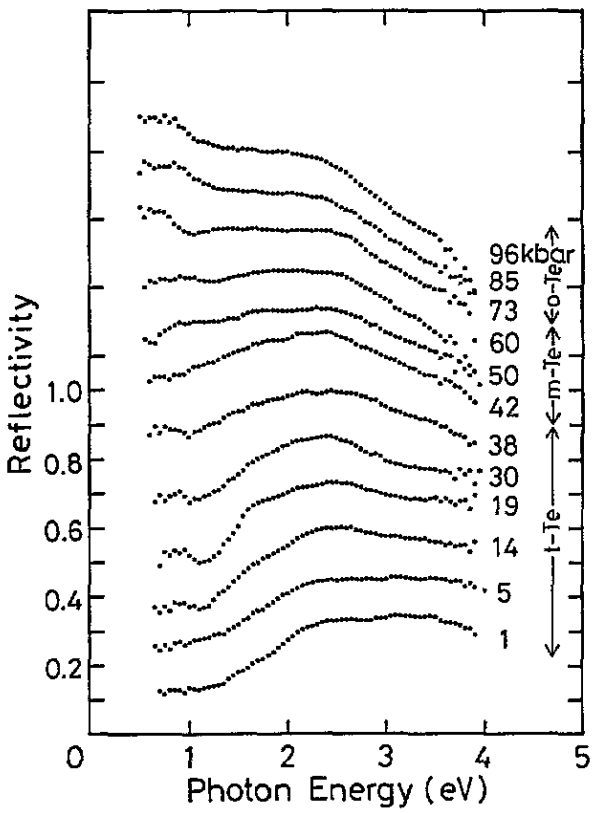

Figure 7. Pressure variation of the reflectivity spectra for trigonal Te (t-Te), monoclinic Te (m-Te) and orthorhombic Te (o-Te). The zero lines of the reflectivity are shifted by 0.1 for each different pressure.

There are different aspects for the various phases of Te. The dotted curves in figure 8 show the reflectivity spectra for the trigonal phase at 1 and 38 kbar, for the monoclinic phase at 50 kbar and for the orthorhombic phase at 73 kbar. In the figure the fitting curves calculated using the oscillator fitting method are shown by full curves. The reflectivity at 1 kbar is relatively small (about 0.1) in the near-infrared (NIR) region, rises near 1.3 eV with increasing photon energy and has a broad peak around 3.0 eV, which corresponds to a semiconductor-like spectrum. At 38 kbar just below the transition to the metallic state the reflectivity becomes larger over the entire energy region. The broad peak in the visible

† From x-ray diffraction photographs obtained using a diamond anvil cell, the transformations to the monoclinic phase and the orthorhombic phase were confirmed.

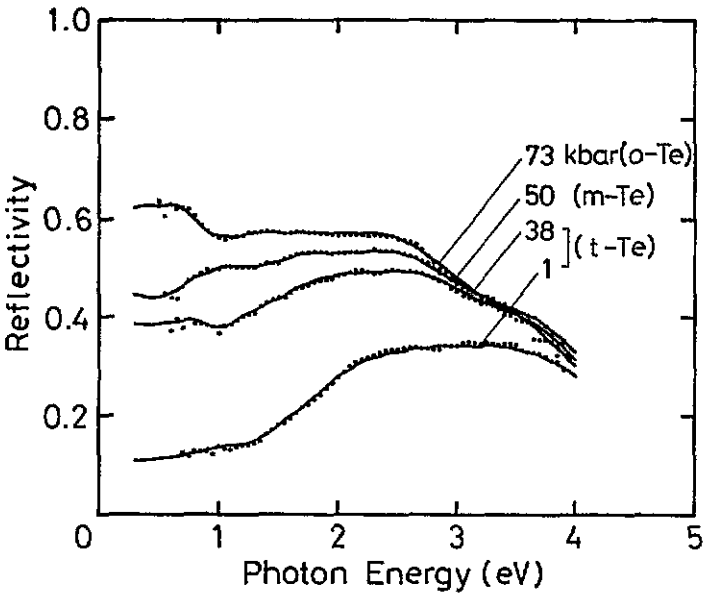

Figure 8. Typical reflectivity spectra for t-, m- and o-Te.

region shifts to lower energy. A small dip of the reflectivity near 1.0 eV is observed. At the transition to the metallic state further increase of the reflectivity is observed in the NIR and visible region. For monoclinic Te at 50 kbar there appear two peaks around 1.0 and 2.0 eV. When Te is transformed into the orthorhombic phase, the reflectivity in the NIR region substantially grows and becomes larger than that in the visible region. The reflectivity spectrum of orthorhombic Te shows more or less metallic behaviour. At all pressures the change of the reflectivity near 4 eV in the ultraviolet (UV) region is relatively small.

3.2. Optical conductivity spectra

Figure 9 shows the pressure variation of the optical conductivity spectra $\sigma(\omega)$ of Te derived from the reflectivity spectra shown in figure 7. It should be noted that the zero lines of the ordinate are shifted by 4000 Ω^{-1} cm^{-1} for each different pressure. For trigonal Te at 1 kbar a main peak at 2.2 eV and a shoulder around 1.2 eV are observed. The main peak exhibits an asymmetrical shape, tailing on the high-energy side. As a result, the $\sigma(\omega)$ curve at 1 kbar indicates semiconducting behaviour with an optical gap. The main peak and the shoulder shift to lower energy with increasing pressure. At 38 kbar just below the metal transition the main peak is located at 1.4 eV, and the shoulder around 0.8 eV. The growth of the shoulder with pressure is rather more rapid than that of the main peak. The optical gap becomes narrow by applying pressure and becomes almost zero at 38 kbar.

When Te is transformed into the monoclinic phase, the shape of $\sigma(\omega)$ spectra changes substantially compared with that for the trigonal phase. There appear a main peak at 1.0 eV and a shoulder around 1.6 eV at 50 kbar. The DC conductivity has the value of 2000 Ω^{-1} cm^{-1}, indicating that the monoclinic phase is metallic. The main peak and the shoulder shift with further pressure and are located around 0.8 eV and 1.5 eV respectively at 60 kbar. The shift rate of the main peak with pressure is larger than that of the shoulder.

When Te becomes the orthorhombic phase, the main peak and the shoulder shift substantially to lower energy. The main peak is located at 0.5 eV and the shoulder around

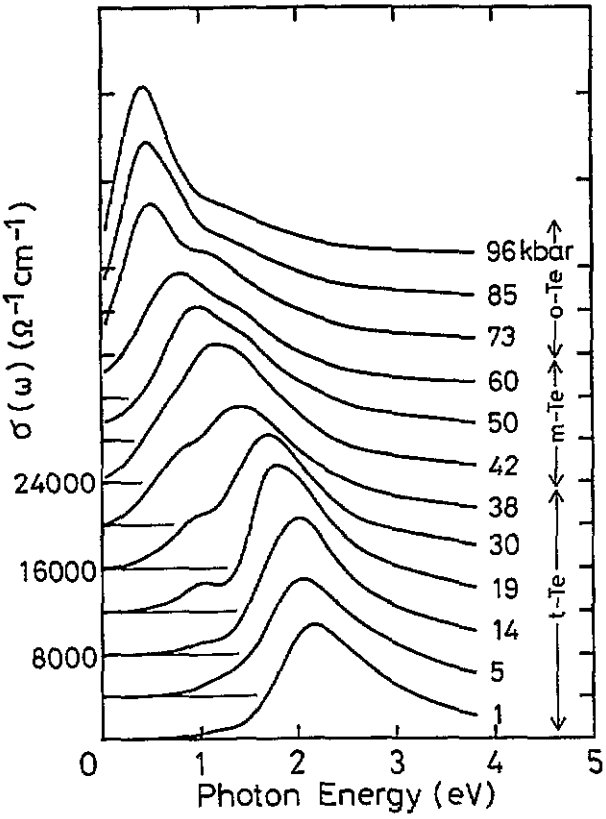

Figure 9. Pressure variation of the optical conductivity spectra $\sigma(\omega)$ of Te up to 96 kbar. The zero lines of the ordinate are shifted by 4000 Ω^{-1} cm^{-1} for each different pressure.

1.2 eV at 73 kbar. Compared with the spectra for monoclinic Te, the intensity of the main peak increases and the half-width of the peak becomes narrow. We can observe the shoulder clearer. With further pressure up to 96 kbar the peak positions of the main peak and the shoulder change little, and the intensity of the main peak increases.

4. Discussion

At 1 kbar, a main peak at 2.2 eV and a shoulder around 1.2 eV are observed for the $\sigma(\omega)$ spectrum of trigonal Te as shown in figure 9. The main peak and the shoulder shift to lower energy with increasing pressure and are located around 1.4 and 0.8 eV respectively at 38 kbar. The results of the band calculation for trigonal Te suggest that these peaks are assigned to the optical transitions from lone-pair (LP) orbitals to σ^* antibonding orbitals [8, 24–26]. Interchain distance decreases substantially with pressure, which is accompanied by the contraction of the a axis perpendicular to spiral chains as seen in figure 2. The increase of interchain coupling causes frequent charge transfer from LP orbitals to σ^* orbitals in the neighbouring chain, which weakens covalent bonds within chains. The weakening of covalent bonds is associated with the result that the length of the c axis parallel to the chains elongates with pressure as shown in figure 2. Since the overlaps of LP orbitals with LP and σ orbitals in the neighbouring chain increase by compression, the width of LP bands

broadens. As a result, the transition energies from LP to σ^* bands decrease. The rapid growth of the shoulder with pressure has been discussed by Starkloff and Joannopoulos [8]. They pointed out that this shoulder particularly originates from the optical transition from the top of LP bands to the bottom of σ^* bands near the M point in the Brillouin zone. The M point is located on the symmetry axis with $k \perp k_z$ components, which is sensitive to the interchain interaction. The rapid growth of the shoulder may imply the substantial increase of the interchain interaction. The theoretical study by Isomaki and Boehm [10] also predicts that the main peak and the shoulder shift to lower energy, and the shoulder grows rapidly with increasing pressure.

The axial ratio c/a of trigonal Te increases by applying pressure, and the transition to the monoclinic phase occurs when c/a increases up to 1.42. It is instructive to note that the transition occurs at nearly the same axial ratio over the whole concentration range of Te_xSe_{1-x} mixtures [3, 6, 27]. The transition may be accomplished without breaking any covalent bonds in trigonal Te [16]. Since the energy difference between helical and planar conformations is small [28–30], the modifications to the helicity along chains, namely rotating two atoms in alternating unit cells along the c axis by $\pi/3$, easily allow the chains to flatten out in a zig-zag pattern as seen in the bc plane of figure 1(b). The transition to the planar zig-zag chain structure may be driven by the bond weakening with pressure.

The $\sigma(\omega)$ spectrum for monoclinic Te at 50 kbar has a main peak at 1.0 eV and a shoulder around 1.6 eV. Furthermore a Drude term appears in the low-energy region, which supports the suggestion that monoclinic Te is metallic. Doerre and Joannopoulos [16] and Shimoi and Fukutome [17] have calculated independently the band structure for monoclinic Te. Figure 10 shows the result obtained by Doerre and Joannopoulos [16]. Along the Γ to X direction four bands cross the Fermi level, decreasing rapidly in energy towards X. This suggests that broadened p-like states are formed along the a axis, and metallic conduction appears along this direction. On the other hand, the bands along the Γ to Y direction and the Γ to Z direction are associated with covalent bonds of two different lengths, namely short bonds and long bonds, which comprise the zig-zag chains. Each band separates into σ_S, σ_L, σ_L^* and σ_S^* bands in order of low energy. Here subscript S and L denote the short bonds and the long bonds respectively. The Fermi level is located between σ_L^* and σ_S^* bands. From the results of these band calculations the main peak at 1.0 eV and the shoulder at 1.6 eV are ascribed to the optical transitions from σ_L^* orbitals to σ_S^* orbitals. Subsequent optical transition is the σ_L to σ_S^* transition, which is about 4 eV apart. The corresponding energy is beyond our measured energy range.

Recently Ikawa [31] has carried out the calculation of $\sigma(\omega)$ spectra as well as the band calculation for monoclinic Te by an empirical pseudopotential method. In figure 11 our $\sigma(\omega)$ spectrum at 50 kbar is compared with the result by Ikawa. The calculated spectrum has a main peak at 1.0 eV and a shoulder around 1.5 eV. Our experimental spectrum is in good agreement with the calculated one. According to Ikawa, the main peak at 1.0 eV is assigned to the σ_L^* to σ_S^* optical transition, which is observed on the way from Γ to Z direction in the band structure of figure 10. It is also identified that the shoulder at 1.5 eV arises from the σ_L^* to σ_S^* transition near the Y point. These positions of the transitions are denoted by arrows in figure 10. The calculated spectrum has small peaks in the 2–3 eV region. However, it is impossible to confirm the presence of these peaks clearly within the present experimental accuracy.

As shown in figure 3, the lattice constants of monoclinic Te change greatly by applying pressure, i.e. the b axis contracts substantially and the angle β between the a axis and the c axis approaches 90° with pressure. Then the bond lengths of the short bonds and the long bonds, which are 2.80 and 3.10 Å respectively at 45 kbar, become the same (3.04 Å) at

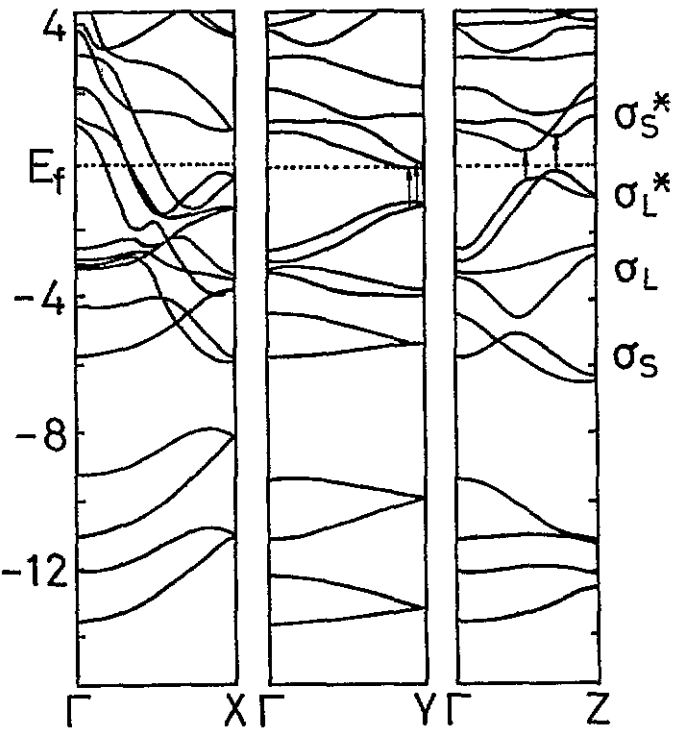

Figure 10. Band structure of monoclinic Te calculated by Doerre and Joannopoulos [16].

68 kbar [5, 6]. For $\sigma(\omega)$ spectra of monoclinic Te we observed that the main peak and the shoulder shift to lower energy with pressure. Ikawa [31] has investigated how $\sigma(\omega)$ spectra are affected by changing the relative lengths of the short and long bonds. He found that the main peak and the shoulder seen in figure 11 shift to lower energy, when the difference in the lengths between the short and long bonds becomes small.

When Te is transformed into the orthorhombic phase, the main peak and the shoulder shift substantially to lower energy. At 73 kbar the main peak is located at 0.5 eV and the shoulder around 1.2 eV. For orthorhombic Te the angle β equals 90° and the lengths of the long bonds and the short bonds are the same as mentioned above. Though the band calculation for orthorhombic Te has not been reported yet, it is expected that the gap between σ_L^* and σ_S^* bands closes. The σ_S and σ_L bands form σ bands, and σ_L^* and σ_S^* bands form σ^* bands. Then the Fermi level is in σ^* bands. The main peak at 0.5 eV and the shoulder at 1.2 eV may be assigned to the optical transitions from occupied σ^* orbitals to unoccupied σ^* orbitals. The band calculation for orthorhombic Te is helpful for understanding the experimental results of $\sigma(\omega)$ spectra in detail.

5. Summary

Reflectivity spectra of Te were measured at pressures up to 96 kbar by using a diamond anvil cell. An oscillator fitting method was applied to derive optical conductivity spectra $\sigma(\omega)$ from the reflectivity.

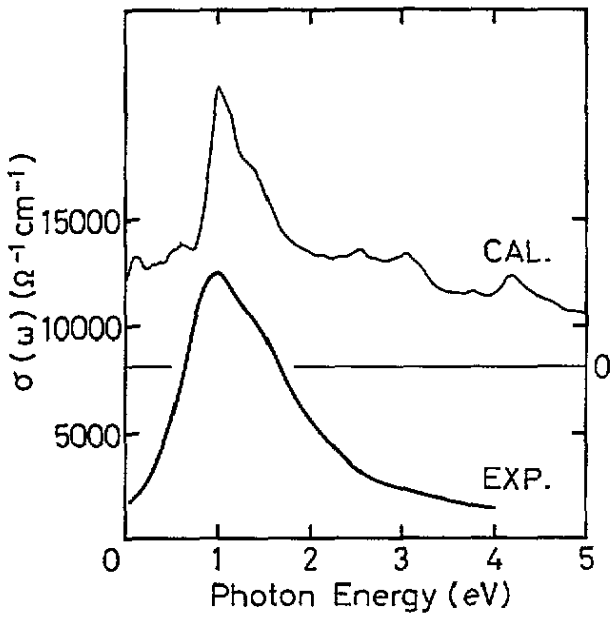

Figure 11. Experimental $\sigma(\omega)$ spectrum for monoclinic Te at 50 kbar and the calculated one by Ikawa [31]. The ordinate of the calculated spectrum is given in arbitrary units.

A main peak at 2.2 eV and a shoulder around 1.2 eV are observed in the $\sigma(\omega)$ spectrum for trigonal Te at 1 kbar, which are assigned to the LP to σ^* optical transitions. The main peak and the shoulder shift to low energy and grow with pressure up to 38 kbar. The shifts and growths of these peaks can be understood by considering the increase of interchain interaction and the weakening of covalent bonds within chains. The $\sigma(\omega)$ spectrum for monoclinic Te at 50 kbar has a main peak at 1.0 eV and a shoulder around 1.6 eV. In addition, a Drude term appears in the low-energy region, suggesting that Te is transformed into a metallic phase. From the results of the band calculation for monoclinic Te, the main peak and the shoulder can be ascribed to the σ_L^* to σ_S^* optical transitions. When Te is transformed into an orthorhombic phase, the main peak and the shoulder shift further to low energy. The main peak is located at 0.5 eV and the shoulder around 1.2 eV at 73 kbar. The main peak and shoulder may be associated with the occupied σ^* to unoccupied σ^* optical transitions.

It is known that Se as well as Te undergoes a pressure-induced semiconductor–metal transition. Reflectivity measurements of Se under pressure are now in progress.

Acknowledgments

The authors would like to thank Dr A Ikawa for discussions concerning his band calculation and for making some results available prior to publication. Our thanks are also due to Professor H Fukutome for his helpful comments. This work was supported by the Grand-in-Aid for Scientific Research Fund from the Ministry of Education, Science and Culture of Japan.

References

[1] Bridgman P W 1945 *Proc. Am. Acad, Arts Sci.* **76** 1
[2] Jamieson J C and McWhan D B 1965 *J. Chem. Phys.* **43** 1149
[3] Keller R, Holzapfel W B and Schulz H 1977 *Phys. Rev.* B **16** 4404
[4] Parthasarathy G and Holzapfel W B 1988 *Phys. Rev.* B **37** 8499
[5] Aoki K, Shimomura O and Minomura S 1980 *J. Phys. Soc. Japan* **48** 551
[6] Ohmasa Y, Yamamoto I and Endo H in preparation
[7] Starkloff T and Joannopoulos J D 1978 *J. Chem. Phys.* **68** 579
[8] Starkloff T and Joannopoulos J D 1979 *Phys. Rev.* B **19** 1077
[9] Isomaki H, von Boehm J, Krusius P and Stubb T 1980 *Phys. Rev.* B **22** 2945
[10] Isomaki H M and von Boehm J 1987 *Phys. Rev.* B **35** 8019
[11] Bridgman P W 1952 *Proc. Am. Acad. Arts Sci.* **81** 167
[12] Matthias B T and Olsen J L 1964 *Phys. Lett.* **13** 202
[13] Blum F A Jr and Deaton B C 1965 *Phys. Rev.* **137** A1410
[14] Bundy F P and Dunn K J 1980 *Phys. Rev. Lett.* **44** 1623
[15] Parthasarathy G, Rao K J and Gopal E S R 1984 *Solid State Commun.* **52** 867
[16] Doerre G and Joannopoulos J D 1979 *Phys. Rev. Lett.* **43** 1040
[17] Shimoi Y and Fukutome H 1992 *Prog. Theor. Phys.* **87** 307
[18] Edwards D F and Philipp H R 1985 *Handbook of Optical Constants of Solids* ed E D Palik (London: Academic) p 665
[19] Syassen K and Sonnenschein R 1982 *Rev. Sci. Instrum.* **53** 644
[20] Welber B 1976 *Rev. Sci. Instrum.* **47** 183
[21] Welber B 1977 *Rev. Sci. Instrum.* **48** 395
[22] Ikemoto H, Yamamoto I, Yao M and Endo H 1994 *J. Phys. Soc. Japan* **63** 1611
[23] Tutihasi S, Roberts G G, Keezer R C and Drews R E 1969 *Phys. Rev.* **177** 1143
[24] Maschke K 1971 *Phys. Status Solidi* b **47** 511
[25] Isomaki H M, von Boehm J and Stubb T 1982 *Phys. Rev.* B **26** 5815
[26] Isomali H M and von Boehm J 1982 *Phys. Scr.* **25** 801
[27] Parthasarathy G and Holzapfel W B 1988 *Phys. Rev.* B **38** 10 105
[28] Springborg M and Jones R O 1988 *J. Chem. Phys.* **88** 2652
[29] Ikawa A and Fukutome H 1989 *J. Phys. Soc. Japan* **58** 4517
[30] Ikawa A and Fukutome H 1990 *J. Phys. Soc. Japan* **59** 4041
[31] Ikawa A private communication